The Astronomical Journal, 171:203 (11pp), 2026 April https://doi.org/10.3847/1538-3881/ae3d9f

TOI-6692 b: An Eccentric 130 Day Period Giant Planet with a Single Transit from TESS

Allyson Bieryla[1,2], Karen A. Collins[1], George Zhou[2], David W. Latham[1], Brad Carter[2], Paul Dalba[3], Robert Gagliano[4], Thomas L. Jacobs[5], Martti Holst Kristiansen[6], Daryll LaCourse[38], Mark Omohundro[7], H.M. Schwengeler[7], Khalid Barkaoui[8,9,10], Rafael Brahm[11,12], R. Paul Butler[13], Douglas A. Caldwell[14,15], Jeffrey D. Crane[16], Tansu Daylan[17], Sarah Deveny[18], Jason D. Eastman[1], Yadira S. Gaibor[19,20], Michaël Gillon[9], Thomas Henning[21], Keith Horne[22], Steve B. Howell[15], Emmanuel Jehin[23], Eric L. N. Jensen[24], Andrés Jordán[11,12], Michelle Kunimoto[25], Colin Littlefield[18], Léna Parc[26], Samuel N. Quinn[1], Malena Rice[27], Joseph E. Rodriguez[28], Richard P. Schwarz[1], Ramotholo Sefako[29], Stephen A. Shectman[16], Avi Shporer[20], Abderahmane Soubkiou[9], Gregor Srdoc[30], Michal Steiner[26], Marcelo Tala Pinto[31], Johanna Teske[13], Trifon Trifonov[21,32,33], Solène Ulmer-Moll[26,34], Cristilyn N. Watkins[35], Sharon X. Wang[36], Jhon Yana Galarza[17,37,39], and Samuel W. Yee[1]
[1] Center for Astrophysics | Harvard & Smithsonian, 60 Garden Street, Cambridge, MA 02138, USA; abieryla@cfa.harvard.edu
[2] University of Southern Queensland, Centre for Astrophysics, West Street, Toowoomba, QLD 4350, Australia
[3] Department of Astronomy and Astrophysics, University of California, Santa Cruz, CA 95064, USA
[4] Amateur Astronomer, Glendale, AZ 85308, USA
[5] Amateur Astronomer, Missouri City, TX 77459, USA
[6] Brorfelde Observatory, Observator Gyldenkernes Vej 7, DK-4340 Tølløse, Denmark
[7] Citizen Scientist, c/o Zooniverse, Department of Physics, University of Oxford, Denys Wilkinson Building, Keble Road, Oxford, OX1 3RH, UK
[8] Instituto de Astrofísica de Canarias (IAC), Calle Vía Láctea s/n, 38200, La Laguna, Tenerife, Spain
[9] Astrobiology Research Unit, Université de Liège, 19C Allée du 6 Août, 4000 Liège, Belgium
[10] Department of Earth, Atmospheric and Planetary Science, Massachusetts Institute of Technology, 77 Massachusetts Avenue, Cambridge, MA 02139, USA
[11] Facultad de Ingeniería y Ciencias, Universidad Adolfo Ibáñez, Av. Diagonal las Torres 2640, Peñalolén, Santiago, Chile
[12] Millennium Institute for Astrophysics, Nuncio Monseñor Sotero Sanz 100, Of. 104, Providencia, Santiago, Chile
[13] Earth and Planets Laboratory, Carnegie Institution for Science, 5241 Broad Branch Road, NW, Washington, DC 20015, USA
[14] SETI Institute, Mountain View, CA 94043, USA
[15] NASA Ames Research Center, Moffett Field, CA 94035, USA
[16] The Observatories of the Carnegie Instution for Science, 813 Santa Barbara Street, Pasadena, CA 91101, USA
[17] Department of Physics and McDonnell Center for the Space Sciences, Washington University, St. Louis, MO 63130, USA
[18] Bay Area Environmental Research Institute, Moffett Field, CA 94035, USA
[19] Department of Physics, Massachusetts Institute of Technology, 77 Massachusetts Avenue, Cambridge, MA 02139, USA
[20] Department of Physics and Kavli Institute for Astrophysics and Space Research, Massachusetts Institute of Technology, Cambridge, MA 02139, USA
[21] Max-Planck-Institut fúr Astronomie, Königstuhl 17, D-69117 Heidelberg, Germany
[22] SUPA Physics and Astronomy, University of St. Andrews, Fife, KY16 9SS Scotland, UK
[23] Space Sciences, Technologies and Astrophysics Research (STAR) Institute, Université de Liège, Allée du 6 Août 19C, B-4000 Liège, Belgium
[24] Department of Physics & Astronomy, Swarthmore College, Swarthmore, PA 19081, USA
[25] Department of Physics and Astronomy, University of British Columbia, 6224 Agricultural Road, Vancouver, BC V6T 1Z1, Canada
[26] Observatoire de Genève, Département d'Astronomie, Université de Genève, Chemin Pegasi 51, 1290 Versoix, Switzerland
[27] Department of Astronomy, Yale University, 219 Prospect Street, New Haven, CT 06511, USA
[28] Center for Data Intensive and Time Domain Astronomy, Department of Physics and Astronomy, Michigan State University, East Lansing, MI 48824, USA
[29] South African Astronomical Observatory, P.O. Box 9, Observatory, Cape Town 7935, South Africa
[30] Kotizarovci Observatory, Sarsoni 90, 51216 Viskovo, Croatia
[31] Department of Astronomy, McPherson Laboratory, The Ohio State University, 140 W 18th Avenue, Columbus, OH 43210, USA
[32] Department of Astronomy, Sofia University "St Kliment Ohridski," 5 James Bourchier Blvd, BG-1164 Sofia, Bulgaria
[33] Landessternwarte, Zentrum für Astronomie der Universität Heidelberg, Königstuhl 12, D-69117 Heidelberg, Germany
[34] Leiden Observatory, Leiden University, P.O. Box 9513, 2300 RA, Leiden, The Netherlands
[35] Bozeman, MT 59718, USA
[36] Department of Astronomy, Tsinghua University, Beijing 100084, People's Republic of China
[37] Departamento de Astronomía, Facultad de Ciencias Físicas y Matemáticas Universidad de Concepción, Av. Esteban Iturra s/n Barrio Universitario, Casilla 160-C, Chile
Received 2025 October 30; revised 2026 January 9; accepted 2026 January 22; published 2026 March 3

Abstract

We report the discovery and characterization of TOI-6692 b, an eccentric ($e \sim 0.54$) Jupiter on a 130 day orbit. TOI-6692 b was first detected as a community TESS Object of Interest by the Visual Survey Group and the Planet Hunters group as a single-transit candidate via TESS observation. The period was subsequently confirmed via radial velocity monitoring from the Planet Finder Spectrograph on the 6.5 m Magellan telescope. Additional radial velocities were acquired with the CHIRON, FEROS, and CORALIE spectrographs. LCOGT ground-based photometric follow-up was conducted over 2 weeks to detect another transit and refine the period. Although we

[38] Amateur Astronomer.
[39] Carnegie Fellow.

did not detect an ingress or egress of the 11.04 hr transit, we did detect a possible in-transit signal in the multinight data and provide an updated ephemeris for future monitoring. TOI-6692 b is one of the few planets with orbital periods longer than 100 days that have a secure mass, radius, and eccentricity detection. As with most giant planets at these orbital periods, the eccentricity of TOI-6692 b is lower than that expected of planets undergoing high-eccentricity tidal migration, but is more consistent with the expectations of planet–planet scattering outcomes. A long-term radial velocity trend was detected, and further monitoring is warranted to determine the outer companion period. TOI-6692 b is also one of the few TESS single transit targets to have its periods eventually confirmed via follow-up photometric campaigns timed to capture transits despite the relatively large ephemeris uncertainties. Such efforts highlight the capabilities of night-to-night stability on ground-based photometric facilities today.

Unified Astronomy Thesaurus concepts: Exoplanet astronomy (486)

1. Introduction

Less than 1% of known giant exoplanets with periods longer than 100 days have had their mass and radius measured.[40] Long-period exoplanets are inherently difficult to confirm. Observationally, transits of long-period planets are geometrically rare, and they require more dedicated time to follow up as a result of the rarity and long duration of their transits. As such, only 15 giant planets with orbital periods >100 days have had their 3σ masses and radii measured. While these cool Jupiter planets are observationally challenging, it is important to invest resources in them. Many such long-period planet candidates from NASA's Transiting Exoplanet Survey Satellite (TESS; G. R. Ricker et al. 2015) exhibit only single-transit detections in the original discovery lightcurves. Following up such single-transit candidates is a technically challenging and resource-intensive exercise. Of the 15 giant planets (listed in Table 1), five are single-transit planet candidates that received campaigns of ground- and space-based follow-up to determine the true periods of the planets.

Hot Jupiters experience high stellar irradiation, which can alter their thermal structure and size. Modeling this "radius anomaly" effect is an active area of research (I. Baraffe & G. Chabrier 2010; G. Laughlin 2018; P. Sarkis et al. 2021). In contrast, long-period giant planets are weakly irradiated and make well-suited laboratories for testing relationships between mass, radius, and metal enrichment (D. P. Thorngren et al. 2016; J. K. Teske et al. 2019). Long-period giant planets that do not empirically show this radius anomaly allow independent investigations of interior structure, metallicity, and planet formation histories (S. Ginzburg & E. Chiang 2020). Additionally, long-period giant planets are testbeds for understanding the formation and evolution of hot Jupiters. They experience little to no tidal disruption, and therefore their dynamical histories are better preserved as compared to their hot Jupiter counterparts.

In this paper, we report the planetary confirmation of TOI-6692 b, a warm Jupiter on a 130 day eccentric orbit ($e \sim 0.54$). Only one transit of TOI-6692 b has been recorded by the NASA TESS mission to date. We conducted a ground-based follow-up campaign that eventually determined the period of the planet via both radial velocity orbit detection and subsequent photometric transit recovery. In Section 2, we describe the photometric data from TESS and the ground-based Las Cumbres Observatory follow-up campaign, high-resolution speckle imaging, and CHIRON, FEROS, CORALIE, and Planet Finder Spectrograph (PFS) spectroscopic observations to obtain a planetary mass. Section 3 describes the global modeling of the system to derive system parameters. We then conclude with a discussion of the system in Section 4.

2. Observations

2.1. Photometric Observations

2.1.1. TESS Photometry

TESS (G. R. Ricker et al. 2015) is performing an all-sky survey in search of transiting exoplanets around nearby bright host stars observing 24° × 96° of the sky during sectors of approximately 27 days. TOI-6692 (TIC 324609409) was observed by TESS in Sector 27 at a cadence of 600 s and in Sectors 39, 66, 67, 93, and 94 at a cadence of 120 s. Data were processed by the NASA Science Processing Operations Center pipeline (SPOC; J. M. Jenkins et al. 2016), and the lightcurves were downloaded from the Mikulski Archive for Space Telescopes[41] using the Lightkurve package (Lightkurve Collaboration et al. 2018). The Presearch Data Conditioning Simple Aperture Photometry (PDCSAP; J. C. Smith et al. 2012; M. C. Stumpe et al. 2012, 2014) lightcurves were used in our analysis and are plotted in Figure 1.

The SPOC pipelines did not identify this target as a TESS Object of Interest (TOI) because only a single transit was observed in the sectors. Citizen scientists from the Visual Survey Group (M. H. K. Kristiansen et al. 2022) identified a single transit in Sector 39 (2021 May 27–June 24) on 2021 August 7 during part of a focused survey for such long-period candidates, which would not have typically triggered a standard pipeline detection. The candidate was also concurrently and independently discovered through manual vetting by the Planet Hunters TESS collaboration (N. L. Eisner et al. 2020) as a Community TOI on 2021 October 14, and on 2023 October 5 it was promoted to a TOI (N. M. Guerrero et al. 2021).

2.1.2. Ground-based Photometric Monitoring Campaign

TOI-6692 b has a transit duration of 11.06 ± 0.24 hr, which is nearly impossible to observe from any single ground-based observatory. Additionally, given that this planet was only observed via a single transit with TESS and the orbital period confirmed through radial velocities (RVs) as part of this work, the uncertainty in predicted future transit times was fairly large. Based on the ephemeris from the global fit (Section 3) using the single TESS transit observation and the radial velocities, the 1σ transit uncertainty at the epoch of our

[40] NASA Exoplanet Archive as of 2025 October 20.

[41] https://mast.stsci.edu/portal/Mashup/Clients/Mast/Portal.html

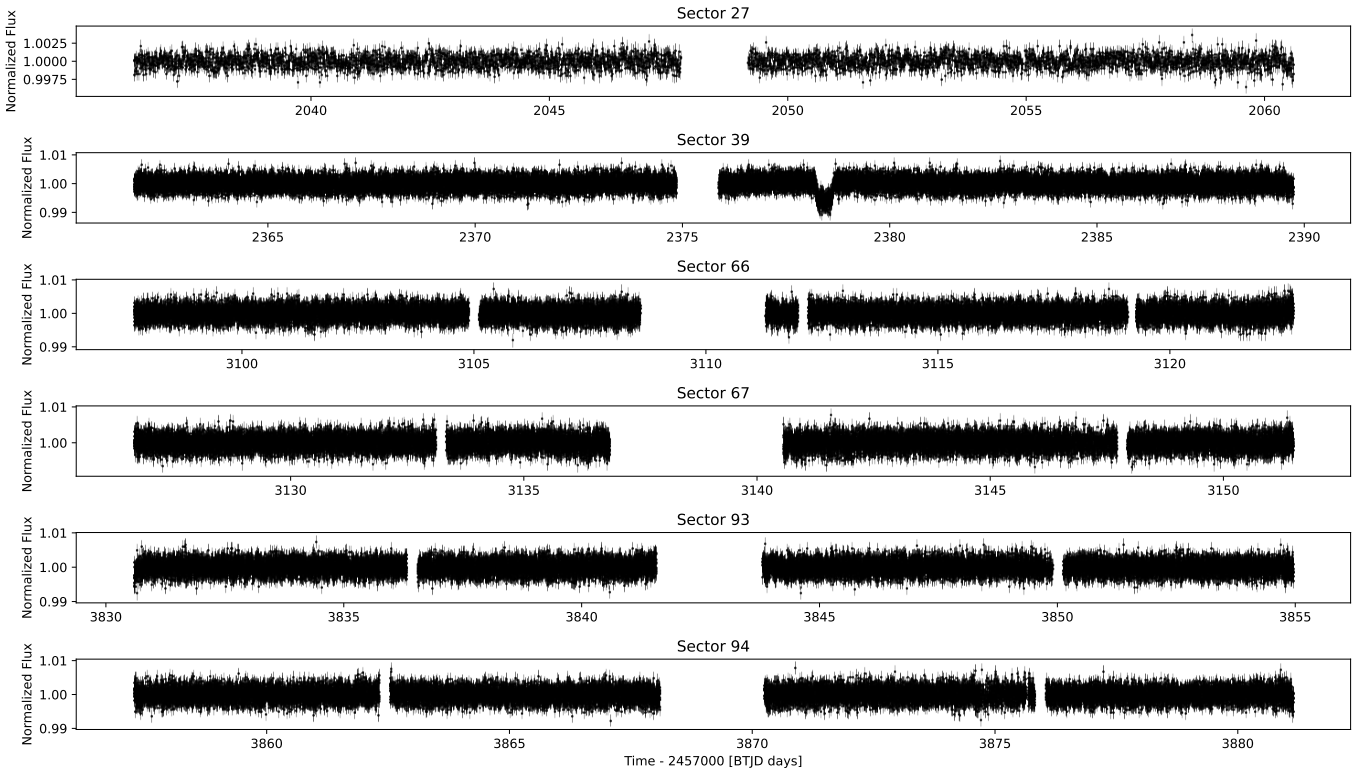

Figure 1. Per-sector normalized TESS PDCSAP lightcurves for TOI-6692. The target star was observed over six TESS sectors. The observing cadence was 600 s in Sector 27 and 120 s in Sectors 39, 66, 67, 93, and 94. Due to the long period, the planet had only a single TESS transit in Sector 39.

Table 1
Confirmed Transiting Planets (6–20 Earth Radii) with 3σ Mass Measurements and Periods Longer than 100 Days

Target	Period (days)	Semimajor Axis (au)	Eccentricity	Radius ($R_{\rm Jup}$)	Mass ($M_{\rm Jup}$)	Known Multiplanet?	Single TESS Transit?	References
Single Star Systems								
TOI-4465 b	101.9	0.416	0.240	1.25	5.89	No	Yes	Z. Essack et al. (2025)
TOI-199 b	104.9	0.425	0.090	0.81	0.17	Yes	Yes	M. J. Hobson et al. (2023)
Kepler 539 b	125.6	0.499	0.390	0.75	0.97	Yes	No	L. Mancini et al. (2016)
TOI-6692 b	**130.57**	**0.512**	**0.537**	**1.04**	**0.62**	**Possible**	Yes	**this work**
KOI-3680 b	141.2	0.534	0.496	0.99	1.93	No	No	G. Hébrard et al. (2019)
TOI-2010 b	141.8	0.552	0.212	1.05	1.29	No	Yes	C. R. Mann et al. (2023)
TIC 241249530 b	165.8	0.641	0.941	1.19	4.98	No	Yes	A. F. Gupta et al. (2024)
Kepler 1514 b	217.8	0.753	0.401	1.11	5.28	Yes	No	P. A. Dalba et al. (2021)
Kepler 111 c	224.8	0.751	0.176	0.63	0.70	Yes	No	P. A. Dalba et al. (2024)
TOI 4562 b	225.1	0.768	0.760	1.12	2.30	Yes	No	A. Heitzmann et al. (2023)
TOI-2180 b	260.8	0.828	0.368	1.01	2.76	No	Yes	P. A. Dalba et al. (2022)
PH 2 b	282.5	0.833	0.215	0.83	0.74	No	No	P. A. Dalba et al. (2024)
Kepler 553 c	328.2	0.898	0.346	1.03	6.70	Yes	No	P. A. Dalba et al. (2024)
Known Multistar Systems								
HD80606 b	111.4	0.457	0.930	1.07	4.38	No	No	D. Naef et al. (2001)
Kepler 35 b	131.5	0.603	0.042	0.73	0.127	No	No	W. F. Welsh et al. (2012)
Kepler 16 b	228.8	0.705	0.007	0.75	0.33	No	No	L. R. Doyle et al. (2011)

Note. TOI-6692 b is highlighted in bold.

ground-based follow-up was −3.9 days and +4.6 days. We alerted the TESS Follow-up Observing Program[42] Sub Group 1 (TFOP; K. Collins 2019) and started monitoring nightly with the Las Cumbres Observatory Global Telescope (LCOGT; T. M. Brown et al. 2013) for 12 days surrounding the nominal predicted ephemeris from the RV orbital solution.

LCOGT is a network of 1 m robotic telescopes equipped with 4096 × 4096 SINISTRO cameras with an image scale of $0\farcs389$ pixel^{-1}, resulting in a $26' \times 26'$ field of view (FOV). We observed six transit attempts at Cerro Tololo Inter-American Observatory in Chile (CTIO), six transit attempts

[42] https://tess.mit.edu/followup

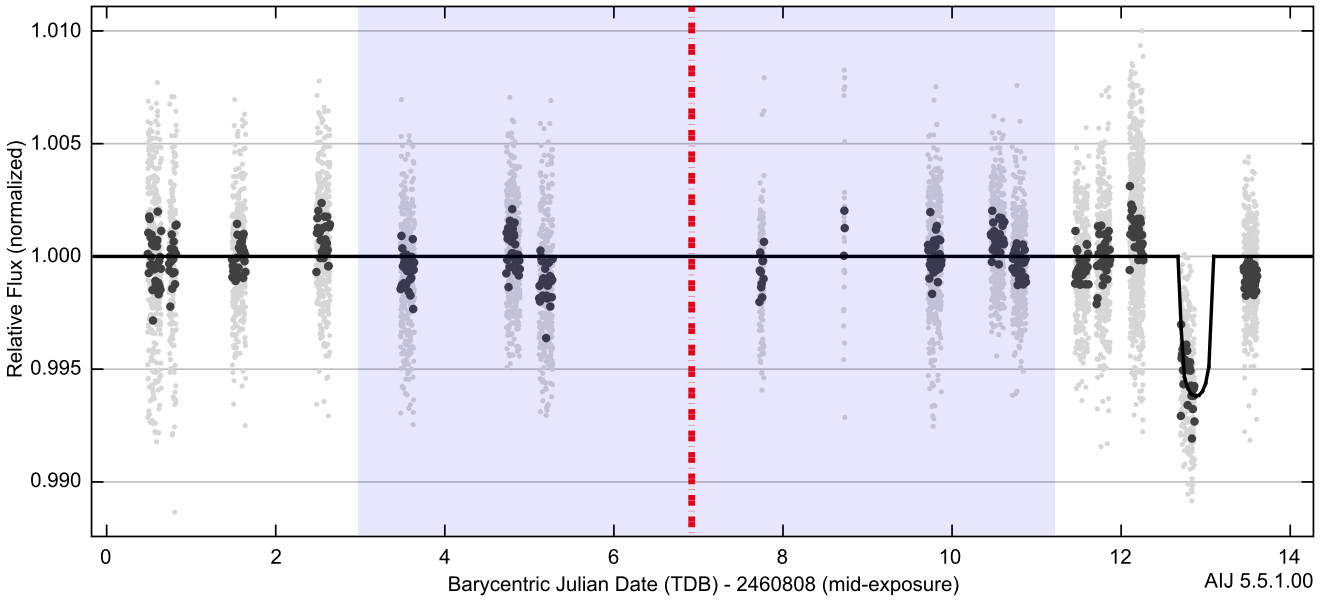

Figure 2. Multinight LCOGT 1.0 m ground-based follow-up lightcurve. The differential lightcurve was extracted using a common set of 22 reference stars and was normalized over the full dataset. No lightcurve detrending was applied. Gray symbols show the unbinned data. Black symbols show the data in 8 minute bins. The vertical red dashed line shows the nominal midtransit time based on the updated ephemeris from the global fit (Section 3), which is based on the single TESS transit detection and all available radial velocities. The blue shaded region indicates the midtransit time 1σ uncertainty window. The apparent 6 ppt in-transit detection is just outside the 1σ window. The bounds on the orbital period based on the TESS single transit, RVs, and the apparent LCOGT in-transit detection are $P = 131.125 \pm 0.012$ days.

Table 2
LCO Ground-based Photometry Campaign

Observatory	Telescope Size (m)	Camera	Filter	Pixel Scale (arcsec)	UT Start Date yyyy-mm-dd	UT Time hh:mm:ss	rms $\mathrm{rms}_{10\mathrm{min}}$ (ppt)
CTIO	1.0	SINISTRO	i'	0.39	2025-05-13	05:43:08–07:52:12	0.69
SAAO	1.0	SINISTRO	i'	0.39	2025-05-13	23:34:00–03:27:25	0.69
SAAO	1.0	SINISTRO	i'	0.39	2025-05-14	23:29:59–03:23:37	0.66
SAAO	1.0	SINISTRO	i'	0.39	2025-05-15	23:26:27–03:20:23	0.67
CTIO	1.0	SINISTRO	i'	0.39	2025-05-17	05:27:30–09:21:17	0.69
SSO	1.0	SINISTRO	i'	0.39	2025-05-17	14:46:19–18:39:47	0.69
CTIO	1.0	SINISTRO	i'	0.39	2025-05-22	05:08:01–09:01:26	0.53
SAAO	1.0	SINISTRO	i'	0.39	2025-05-22	22:58:36–02:52:17	0.51
CTIO	1.0	SINISTRO	i'	0.39	2025-05-23	05:05:30–08:59:18	0.47
SAAO	1.0	SINISTRO	i'	0.39	2025-05-23	22:54:50–02:48:21	0.50
CTIO	1.0	SINISTRO	i'	0.39	2025-05-24	05:00:12–08:53:49	0.71
SSO	1.0	SINISTRO	i'	0.39	2025-05-24	14:24:57–18:18:47	0.76
CTIO	1.0	SINISTRO	i'	0.39	2025-05-25	04:56:18–08:49:56	0.67
SAAO	1.0	SINISTRO	i'	0.39	2025-05-25	22:46:49–02:40:41	0.38

with the South African Astronomical Observatory near Sutherland, South Africa (SAAO), and two transit attempts with the Siding Spring Observatory near Coonabarabran, Australia (SSO). A total of 14 observations were obtained over a 12 day period starting on UT 2025 May 13 (see Table 2). We used the `TESS Transit Finder`, a customized version of the `Tapir` software package (E. Jensen 2013), to automatically schedule ground-based transit observations. All images were calibrated by the standard LCOGT `BANZAI` pipeline (C. McCully et al. 2018). `AstroImageJ` (K. A. Collins et al. 2017) was used to extract the differential aperture photometry.

The time-series coverage of all observations is shown in Figure 2. The 11.04 hr transit duration is longer than the target is observable at any of the observatory locations. Unfortunately, several nights of bad weather occurred near the nominal transit center time prediction. An additional observation was obtained on 2025 May 19 UT with the TRAnsiting Planets and PlanetesImals Small Telescope in the South (TRAPPIST-South). TRAPPIST-South is a 60 cm robotic telescope located at La Silla Observatory in Chile (M. Gillon et al. 2011; E. Jehin et al. 2011). The telescope is equipped with an Andor iKon-L BEX2-DD deep-depletion 2K×2K e2V CCD, resulting in a $20' \times 20'$ FOV and a plate scale of $0\farcs60\,\mathrm{pixel}^{-1}$. Several images in the dataset were saturated, and the observations were taken with a different CCD and filter from the others in this campaign. The TRAPPIST-South observation was excluded from the LCOGT final analysis in order to create a homogeneous set of observations, all taken in the same Sloan i' filter, same telescope size, and same SINISTRO detectors. In addition, we used the same $7\farcs8$ radius

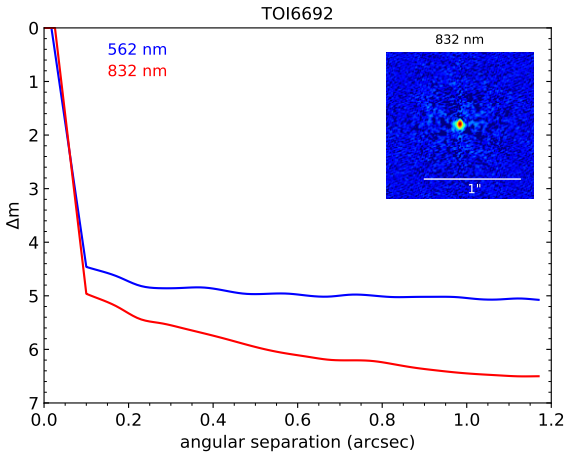

Figure 3. The figure shows 5σ magnitude contrast curves in both filters as a function of the angular separation out to 1.″2. The inset shows the reconstructed 832 nm image of TOI-6692 with a 1″ scale bar. TOI-6692 was found to have no close companions from 0.″1 to 1.″2 to within the magnitude contrast levels achieved.

photometric aperture and a common set of 22 reference stars to extract the combined differential lightcurve.

The combined lightcurve was then normalized as a single lightcurve and no detrending was applied. The resulting lightcurve is shown in Figure 2. There are 1–2 ppt offsets in the night-to-night, telescope-to-telescope baselines, except for an apparent 5–6 ppt offset in the next-to-last observation. This offset could be due to the observation catching an in-transit segment of the expected 6 ppt deep transit. If this segment of data is indeed an in-transit detection, the upper and lower bounds on the orbital period based on the TESS single transit, RVs, and the apparent LCOGT in-transit detection are $P = 131.125 \pm 0.012$ days. The apparent event occurred just beyond the time window of the 1σ upper range, as determined from the global analysis in Section 3.

2.1.3. High-resolution Imaging

Spatially close stellar companions to exoplanet host stars (bound or line of sight) can create a false-positive transit signal and will contribute "Third-light" flux, leading to an underestimated planetary radius (D. R. Ciardi et al. 2015) and incorrect derived parameters for both the host star and the planet if not accounted for (E. Furlan & S. B. Howell 2017; E. Furlan & S. B. Howell 2020). Thus, to search for close-in (bound) companions unresolved in TESS or other ground-based follow-up observations, we obtained high-resolution imaging speckle observations of TOI-6692.

TOI-6692 was observed on 2025 May 10 UT using the Zorro speckle instrument on the Gemini South 8 m telescope (N. J. Scott et al. 2021). Zorro provides simultaneous speckle imaging in two bands (562 and 832 nm) with output data products including a reconstructed image with robust contrast limits on companion detections (e.g., S. B. Howell et al. 2025). Four sets of 1000×0.06 s exposures were collected and subjected to Fourier analysis in our standard reduction pipeline (see S. B. Howell et al. 2011). Figure 3 shows our final contrast curves and the 832 nm reconstructed speckle image. We find that TOI-6692 is a single star with no companion brighter than 5–6.5 mag below that of the target star from 0.″1 out to 1.″2. At the distance of TOI-6692 (313 pc), these angular limits correspond to spatial limits of 30–376 au.

Table 3
PFS Radial Velocities

Time (BJD_{TDB})	Velocity ($m\ s^{-1}$)	Uncertainty ($m\ s^{-1}$)
2459717.91484	17.92	4.26
2459796.68778	18.94	4.28
2459834.59932	−5.49	5.20
2459834.60691	−2.01	6.68
2459853.55921	11.23	3.93
2459855.53952	18.72	4.17
2459889.52721	56.80	3.75
2459893.53582	56.52	4.90
2459895.54528	31.51	4.60
2460065.89343	15.00	3.96
2460065.90388	4.58	3.91
2460067.89668	−5.37	4.88
2460067.90752	6.71	4.63
2460072.89346	−10.69	4.28
2460072.90625	2.98	4.39
2460073.90792	14.11	4.23
2460073.91849	8.69	3.77
2460074.89392	10.05	4.09
2460074.90508	−6.84	3.81
2460122.76347	−9.90	4.86
2460122.77463	−4.70	4.74
2460126.79969	−5.89	4.03
2460126.81056	13.39	3.90
2460153.74789	53.08	4.10
2460180.64172	11.78	3.70
2460210.67252	−12.13	4.07
2460459.84529	−16.20	3.52
2460461.85411	−13.58	5.26
2460463.83988	−11.31	3.26
2460464.85629	−11.02	3.27
2460485.79046	−25.97	4.17
2460488.84101	−18.70	3.62
2460490.77108	−4.65	3.35
2460492.77987	−8.22	3.25
2460509.75949	−7.42	3.27
2460510.71692	−5.08	3.79
2460516.71909	5.29	3.99
2460517.72135	0.00	4.11
2460536.67995	36.43	3.78
2460544.67713	33.60	3.86
2460596.54190	−14.47	3.39
2460805.90984	24.70	3.84
2460810.89294	12.61	3.50
2460834.84703	−10.91	3.87
2460843.82105	−5.51	4.30

2.2. Spectroscopic Observations

A total of 89 spectra from four observatories were obtained between UT 2021 September 13 and 2025 June 17 to measure the stellar parameters of the star and to measure a mass of the companion. Information about the facilities and observations is described in the following subsections.

2.2.1. CHIRON

CHIRON is a fiber-fed echelle spectrograph on the 1.5 m SMARTS telescope at Cerro Tololo Inter-American Observatory, Chile (A. Tokovinin et al. 2013). CHIRON observes over the wavelength range 4100–8200 Å and has a spectral resolving power of $R \sim 80{,}000$. Spectra were extracted as per the official CHIRON pipeline

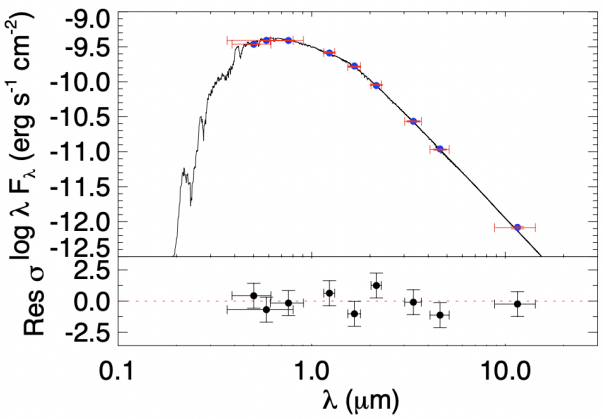

Figure 4. Spectral energy distribution of the target star TOI-6692. Magnitudes from Gaia G, B_p, and R_p, 2MASS J, H, and Ks, and WISE W1, W2, W3, and W4 are included in the global modeling of the system and are shown in dark blue.

Table 4
Literature Values for TOI-6692

Stellar Parameters	Value	Source
Catalog Information		
TIC ID	TIC 324609409	TOI Catalog
TOI ID	TOI-6692	TOI Catalog
Gaia DR3 ID	6349145498210403840	GAIA DR3
2MASS ID	J20504634-8116202	2MASS
TYC ID	9473-00833-1	Tycho
Coordinates and Proper Motion		
R.A. (h:m:s)	20:50:46.57 (J2000)	GAIA DR3
decl. (d:m:s)	−81:16:20.63 (J2000)	GAIA DR3
Parallax (mas)	3.2203 ± 0.0119	GAIA DR3
$\mu_{R.A.}$ (mas yr^{-1})	38.7968 ± 0.0128	GAIA DR3
$\mu_{Dec.}$ (mas yr^{-1})	−22.7508 ± 0.0128	GAIA DR3
Magnitudes		
TESS (mag)	11.116 ± 0.006	TOI Catalog
G (mag)	11.578162 ± 0.002762	GAIA DR3
B_p (mag)	11.932896 ± 0.002829	GAIA DR3
R_p (mag)	11.050061 ± 0.003797	GAIA DR3
B (mag)	12.305 ± 0.209	Tycho
V (mag)	11.434 ± 0.016	Tycho
J (mag)	10.432 ± 0.023	2MASS
H (mag)	10.136 ± 0.022	2MASS
K (mag)	10.034 ± 0.019	2MASS
WISE$_{3.4\mu}$ (mag)	10.029 ± 0.023	WISE
WISE$_{4.6\mu}$ (mag)	10.053 ± 0.020	WISE
WISE$_{12\mu}$ (mag)	10.010 ± 0.046	WISE

Note. Source column references are TESS TOI Primary Mission Catalog (N. M. Guerrero et al. 2021); Tycho (E. Høg et al. 2000); GAIA DR3 (Gaia Collaboration et al. 2023); 2MASS (R. M. Cutri et al. 2003); WISE (R. M. Cutri et al. 2021).

(L. A. Paredes et al. 2021). Thirty-one observations were obtained between 2021 September and 2022 September.

2.2.2. FEROS

The Fiber-fed Extended Range Optical Spectrograph (FEROS; A. Kaufer et al. 1999) is a high-resolution, temperature stabilized echelle spectrograph installed at the MPG-2.2 m telescope in the ESO La Silla Observatory in Chile. FEROS has a resolving power of 48,000 and uses a second fiber to trace instrumental wavelength shifts. A total of six observations were obtained

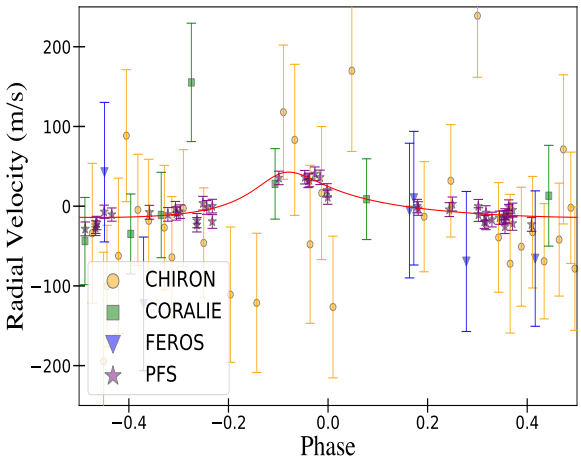

Figure 5. Radial velocity observations phase folded to the ephemeris. The red line shows the EXOFASTv2 best model fit to the RVs. Section 2.2 details the radial velocity observations.

between 2023 August and 2024 June. All reduction and processing steps were performed using the ceres pipeline (R. Brahm et al. 2017).

2.2.3. CORALIE

CORALIE (A. Baranne et al. 1996; D. Queloz et al. 2000; D. Ségransan et al. 2010) is a fiber-fed echelle spectrograph installed on the Swiss 1.2 m Leonhard Euler Telescope at the La Silla Observatory in Chile. It has a spectral resolving power of $R \sim 60{,}000$ and operates in the wavelength range 390–680 nm. We observed TOI-6692 with the first fiber, and we used the second fiber to observe the simultaneous Fabry–Pérot etalon for drift calibration purposes. A total of seven spectra with an exposure time of 1800 s were obtained between 2024 April and July. The spectra were reduced with the standard data reduction pipeline. The radial velocity measurements were obtained by cross correlating each spectrum with a G2-type stellar mask (e.g., F. Pepe et al. 2002).

2.2.4. PFS

The PFS (J. D. Crane et al. 2006, 2008, 2010) is a high-precision spectrograph on the 6.5 m Magellan II Telescope at Las Campanas Observatory in Chile. A total of 45 spectra were obtained between 2022 May and 2024 June, and are listed in Table 3. The spectra were reduced using the methods outlined in R. P. Butler et al. (1996). The spectra were collected using a 0.″3 wide slit, 3 × 3 binning, and 1200 s exposures. The spectral resolving power in this configuration is $R \sim 115{,}000$.

2.3. SED Analysis

All available broadband photometry, including Gaia DR3 G, Bp, and Rp (Gaia Collaboration et al. 2023), Two Micron All Sky Survey (2MASS) J, H, and K (M. F. Skrutskie et al. 2006), and Wide-field Infrared Survey Explorer (WISE) W_1, W_2, and W_3 bands (R. M. Cutri et al. 2021), as well as the Gaia DR3 parallax, were used to construct the spectral energy distribution (SED) of TOI-6692. The SED was modeled simultaneously with the photometric and spectroscopic observations of the system, which is discussed in the next section. The

Table 5
Best-fit Stellar and Planetary Properties for TOI-6692

Parameters	Description (Units)	Prior Values	Best Fit
Stellar Parameters			
$M_\star$	Stellar mass ($M_\odot$)	Inferred	$1.047^{+0.089}_{-0.071}$
$R_\star$	Stellar radius ($R_\odot$)	Inferred	$1.385^{+0.054}_{-0.052}$
$L_\star$	Stellar luminosity ($L_\odot$)	Inferred	2.08 ± 0.20
$T_{\rm eff}$	Effective temperature (K)	Inferred	5890^{+170}_{-180}
$\log g$	Surface gravity (cgs)	Inferred	$4.176^{+0.054}_{-0.051}$
[m/H]	Metallicity (dex)	$\mathcal{G}$(-0.1,0.06)	$-0.008^{+0.030}_{-0.027}$
Parallax	Parallax (mas)	$\mathcal{G}$(3.220,0.012)	3.220 ± 0.012
Age	Age (Gyr)	Inferred	$7.8^{+3.1}_{-3.0}$
Distance	Distance (pc)	Inferred	$310.5^{+1.2}_{-1.1}$
A_V	V-band extinction (mag)	$\mathcal{U}$(0.00, 0.48)	$0.29^{+0.11}_{-0.13}$
Planetary Parameters			
P	Orbital period[a] (days)	Inferred	$130.57^{+0.42}_{-0.35}$
$P_{\rm updated}$	Updated orbital period[b] (days)	Inferred	131.125 ± 0.012
T_0	Epoch (BJD)	$\mathcal{U}$(2459378.4,2459378.5)	2459378.4174 ± 0.0022
M_p	Planet mass ($M_{\rm Jup}$)	Inferred	$0.620^{+0.080}_{-0.065}$
R_p	Planet radius ($R_{\rm Jup}$)	Inferred	$1.042^{+0.050}_{-0.049}$
$a/R_\star$	Semimajor axis to star radius ratio	Inferred	$79.5^{+4.2}_{-3.9}$
a	Semimajor axis (au)	Inferred	$0.512^{+0.014}_{-0.012}$
e	Eccentricity	Inferred	0.537 ± 0.061
ω_*	Arg of periastron (deg)	Inferred	$-16.6^{+7.9}_{-7.7}$
$T_{\rm eq}$	Equilibrium temp[c] (K)	Inferred	$467.0^{+9.3}_{-9.5}$
T_{14}	Transit duration (hr)	Inferred	11.06 ± 0.24
K	RV semiamplitude (m s^{-1})	Inferred	$28.5^{+3.2}_{-2.7}$
$\dot{\gamma}$	RV slope[d] (m s^{-1} day^{-1})	Inferred	$-0.0280^{+0.0046}_{-0.0045}$
i	Orbital inclination (deg)	Inferred	$89.483^{+0.083}_{-0.074}$
b	Impact parameter	Inferred	$0.618^{+0.072}_{-0.120}$

Notes.
[a] Derived from global analysis (Section 3).
[b] Updated based on the ground-based lightcurve detection (Section 2.1.2).
[c] Assumes no albedo and perfect redistribution.
[d] Reference epoch = 2460157.211885.

best-fit model is shown in Figure 4 and the catalog parameters are reported in Table 4.

3. Global Modeling

We performed a joint analysis using EXOFASTv2 (J. Eastman et al. 2013; J. D. Eastman et al. 2019) to determine the stellar and planetary parameters of the system. We incorporated the TESS photometry, all available radial velocities from PFS, CHIRON, FEROS, and CORALIE, and catalog observations to simultaneously fit the system. EXOFASTv2 is an open-source code written in IDL that uses Markov Chain Monte Carlo to derive stellar and planetary parameters. Gaussian priors were adopted for the parallax obtained from GAIA Data Release 3 (GAIA DR3; Gaia Collaboration et al. 2023), which was corrected by L. Lindegren et al. (2021). The starting values for the transit epoch, T_c, and the period, P, were set from the orbital fit of the radial velocities, and the initial starting values on the stellar mass, M_*, and radius, R_*, were obtained from the TESS mission input catalog (K. G. Stassun et al. 2018). We also set a Gaussian prior on metallicity derived from a SpecMatch-Synth stellar parameter analysis (E. A. Petigura 2015) of the iodine-free PFS template spectrum. In brief, SpecMatch-Synth matches the observed spectrum with the R. L. Kurucz (1993) grid of synthetic stellar spectra. The code interpolates between the nearest grid spectra by taking linear combinations to obtain the final spectroscopic parameters. We measured a slightly subsolar metallicity for TOI-6692 of [Fe/H] $= -0.10 \pm 0.06$ dex from this analysis.

We note that the CHIRON, CORALIE, and FEROS RVs have much lower precision than the PFS RVs, as shown in Figure 5. We opted to run comparison fits to ensure that the lower-precision RVs were not degrading the result. In both fits, we included the TESS photometry and all available catalog observations as noted above. We found that in both fits, the stellar and planetary parameters agreed within 1σ. Therefore, we concluded that the lower-precision RVs did not degrade the fit, and we included them in the fit that we adopted as our final results. Those results are listed in Table 5, which also lists the prior values used. Each fit also allowed for a long-term linear trend of $-0.0280^{+0.0046}_{-0.0045}$ m s^{-1} day^{-1}, as shown in Figure 6. This indicates that there may be an unresolved long-period companion in the system. We also ran a comparison two-planet model to check if the second companion's orbital period could be constrained. ΔBIC preferred the single-planet plus RV trend model. We detect no additional periodic transits in the photometry, nor do we detect any companions in the high-resolution imaging. Companion threshold detection limits are described in more detail in the Discussion.

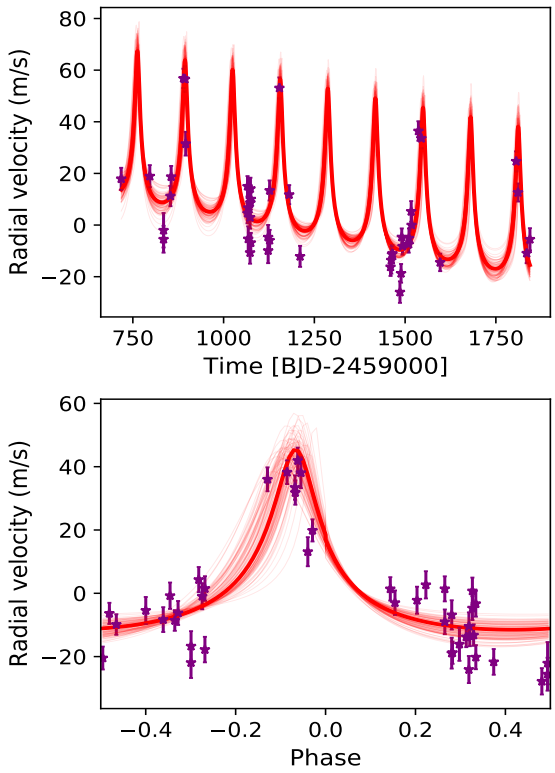

Figure 6. Top: a linear slope showing the PFS radial velocities over time. The trend is detected at $-0.0280^{+0.0046}_{-0.0045}$ m s^{-1}day^{-1}. Longer-term monitoring is necessary to confirm the orbital period of the outer companion. Bottom: PFS radial velocity observations phase folded to the ephemeris for better clarity. The solid, bold, red line is the best-fit model from EXOFASTv2 using RVs from all four facilities. The finer red lines show a small selection of draws from the converged posterior. Section 2.2 details the radial velocity observations.

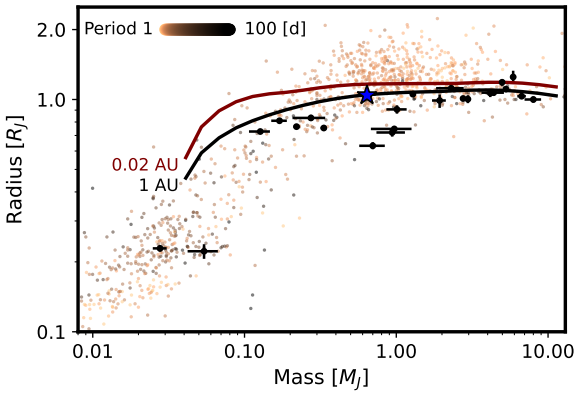

Figure 7. Planet mass versus planet radius for all planets with 3σ mass and radii measurements. Planets with an orbital period $\geqslant$100 days are plotted and shown in black with their respective error bars. Data were obtained on 2025 August 4 from the NASA Exoplanet Archive. TOI-6692 b is shown as a blue star with black edges, and the solid lines show the 10 M_E core (J. J. Fortney et al. 2007) giant planet thermal and atmospheric models at 1 au (in black) and at 0.02 au (in red).

We did not include the ground-based photometric follow-up data in the global fits because the detection is an in-transit event and the data have gaps in time. A global fit that included this data would be very time intensive and not well constrained due to the lack of ingress or egress detected. We instead describe our photometric analysis in Section 2.1.2 and provide an alternative updated period from this analysis for reference.

4. Discussion

TOI-6692 b is a long-period Jupiter-mass planet in an eccentric ($e \sim 0.54$) orbit. Only 15 giant planets have masses and radii measured (at $>3\sigma$ significance) with periods longer than 100 days (Table 1). Figures 7 and 8 place TOI-6692 b into context in the mass, radius, period, and eccentricity space.

TOI-6692 b is part of a dynamically complex, long-period, Jupiter-like system. The planet has an eccentric orbit with a period of 130 days and an eccentricity of 0.537 ± 0.061. PFS radial velocities detect a $\sim$20 m s^{-1} long-term linear trend over a baseline of $\sim$800 days. We combine the radial velocities and the limiting thresholds from speckle imaging to determine constraints on the mass and separation of this exterior companion. We simulate the Keplerian orbit of the exterior companion, and model its I magnitude via the MIST isochrones (A. Dotter 2016). We adopt a distance of 310.5 pc in these calculations as per the Gaia parallax. The modeled Keplerian orbit is matched against the PFS velocity residuals after the removal of TOI-6692 b. The luminosity of the companion and its semimajor axis were checked against the speckle imaging threshold in Section 2.1.3.

Figure 9 shows the constraints that we can place on this exterior companion. We place an upper mass limit of the companion at $\sim$400 M_J, from the speckle imaging observations at orbital distances $>$20 au. Interior to this, the constraints are dominated by the radial velocities.

The eccentricity of TOI-6692 b is similar to that of other recent long-period giant planet discoveries from TESS and Kepler (G. Hébrard et al. 2019; C. R. Mann et al. 2023). As per Figure 8, at such large orbital separations, the eccentricity is not shaped by tidal circularization, and the planet is not expected to follow a high-eccentricity inward-migration track. In fact, among the transiting long-period ($P > 100$ days) planets, only HD80606 b (D. Naef et al. 2001; J. N. Winn et al. 2009) and TIC241249530b (A. F. Gupta et al. 2024) follow the classical high-eccentricity migration track. A significantly larger population of planets has mild eccentricities $<$0.8. E. B. Ford & F. A. Rasio (2008) demonstrate that planet–planet scattering processes yield eccentricities no larger than $e \sim 0.8$, and TOI-6692 b is most consistent with migration via this process (e.g., F. A. Rasio & E. B. Ford 1996; S. Chatterjee et al. 2008; M. Nagasawa et al. 2008).

Figure 7 shows TOI-6692 b on the mass–radius distribution of giant planets, highlighting planets with periods $>$ 100 days. These planets receive mild irradiation compared to conventional hot Jupiters, and are excellent tests of traditional mass–radius relationships for giant planets. The mass and radius of TOI-6692 b is in excellent agreement with model predictions from J. J. Fortney et al. (2007). The role tidal heating plays in retaining internal heat and an "inflated" radius of some planets remains unclear, but atmospheric studies have shown that some low-density giant planets exhibit methane quenching in their atmospheres, suggesting significant interior heating (e.g., D. K. Sing et al. 2024). At transit, TOI-6692 b is at a separation of 0.32 au, with an equilibrium temperature of $\sim$600 K. At this temperature, methane should be a significant absorber at equilibrium. TOI-6692 b has a transmission spectroscopic metric (TSM) of 23 (E. M. R. Kempton et al. 2018). Among planets with similar irradiation, only four other giant planets have higher TSMs. These planets may serve as excellent laboratories for understanding the chemical composition of cold-but-accessible giant planets, to serve

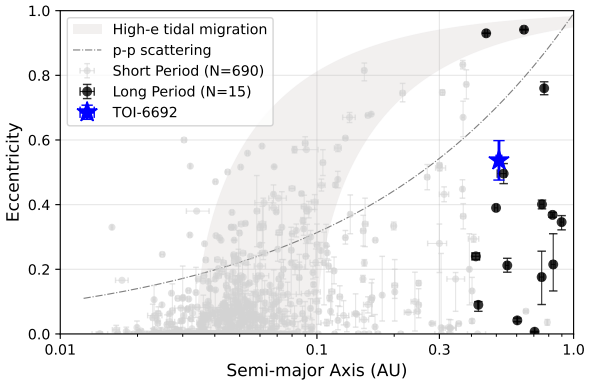

Figure 8. All transiting exoplanets in the range of 6–20 Earth radii. Planets with periods less than 100 days are plotted in light gray, and the 16 planets with periods longer than 100 days are plotted in black. TOI-6692 b is plotted as a blue filled star. The gray region illustrates planets that are likely undergoing high-eccentricity tidal migration. The upper and lower limits of the track are set by the Roche limit and the tidal circularization timescale (J. Dong et al. 2021). The dotted–dashed line presents the theoretical upper limit of eccentricities as a result of planet–planet scattering, assuming a planet with a mass of 0.5 $M_{\rm Jup}$ and a radius of 2 $R_{\rm Jup}$, for illustrative purposes (C. Petrovich et al. 2014). Data were obtained on 2025 August 4 from the NASA Exoplanet Archive.

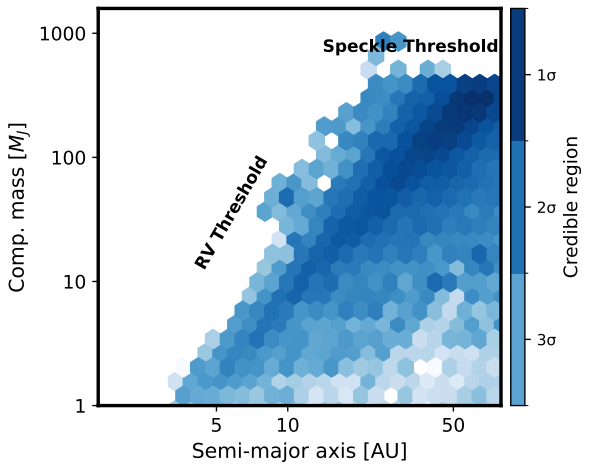

Figure 9. Limits on the properties of the exterior companion that we can place via PFS radial velocities and speckle imaging observations. The exterior companion is limited to 400 M_J in mass from the speckle observations at ∼20 au, and by radial velocities for interior orbital solutions.

as comparisons against similar planets closer in that may exhibit disequilibrium due to added internal heating or photochemistry.

TOI-6692 b demonstrates the challenges associated with confirming long-period, single-transit planet candidates from TESS. While some constraints can be placed from single transits on the orbital period of systems based on the transit duration, the uncertainties are very large. It requires a significant investment of telescope time to confirm the true period. In particular, high-precision radial velocity and photometric follow-up resources are limited. In the case of TOI-6692 b, once we confirmed the period and eccentricity with the radial velocity follow-up, we were then able to utilize the strength of the TFOP SG1 photometric resources and, in particular, the LCO global network of 1 m telescopes to observe the second transit and further refine the period. Similar efforts confirmed the transit of the $P = 542$ day planet HIP 41378 f (J. García-Mejía et al. 2025), the transit of TOI-2010 b via space-based small-sat observations (C. R. Mann et al. 2023), and the NGTS recovery of TIC238855958b (S. Gill et al. 2020).

Acknowledgments

We respectfully acknowledge the traditional custodians of the lands on which we conducted this research and throughout Australia. We recognize their continued cultural and spiritual connection to the land, waterways, cosmos, and community. We pay our deepest respects to all Elders, present and emerging people of the Giabal, Jarowair, and Kambuwal nations, upon whose lands this research was conducted. G.Z. acknowledges the support of the ARC Future Fellowship program FT230100517. Funding for the TESS mission is provided by NASA's Science Mission Directorate. We acknowledge the use of public TESS data from pipelines at the TESS Science Office and at the TESS Science Processing Operations Center. This research has made use of the Exoplanet Follow-up Observing Program website, which is operated by the California Institute of Technology, under contract with the National Aeronautics and Space Administration under the Exoplanet Exploration Program. Resources supporting this work were provided by the NASA High-End Computing (HEC) Program through the NASA Advanced Supercomputing (NAS) Division at Ames Research Center for the production of the SPOC data products. This paper includes data collected by the TESS mission that are publicly available from the Mikulski Archive for Space Telescopes (MAST). This work has made use of data from the European Space Agency (ESA) mission Gaia (https://www.cosmos.esa.int/gaia), processed by the Gaia Data Processing and Analysis Consortium (DPAC, https://www.cosmos.esa.int/web/gaia/dpac/consortium). Funding for the DPAC has been provided by national institutions, in particular the institutions participating in the Gaia Multilateral Agreement. The Flatiron Institute is a division of the Simons Foundation. This work makes use of observations from the LCOGT network. Part of the LCOGT telescope time was granted by NOIRLab through the Mid-Scale Innovations Program (MSIP). MSIP is funded by NSF. Some of the observations in this paper made use of the High-Resolution Imaging instrument Zorro and were obtained under Gemini Proposal Number: GS-2025A-DD-101. Zorro was funded by the NASA Exoplanet Exploration Program and built at the NASA Ames Research Center by Steve B. Howell, Nic Scott, Elliott P. Horch, and Emmett Quigley. Zorro was mounted on the Gemini South telescope of the international Gemini Observatory, a program of NSF's NOIRLab, which is managed by the Association of Universities for Research in Astronomy (AURA) under a cooperative agreement with the National Science Foundation on behalf of the Gemini partnership: the National Science Foundation (United States), National Research Council (Canada), Agencia Nacional de Investigación y Desarrollo (Chile), Ministerio de Ciencia, Tecnología e Innovación (Argentina), Ministério da Ciência, Tecnologia, Inovações e Comunicações (Brazil), and Korea Astronomy and Space Science Institute (Republic of Korea). Funding for K.B. was provided by the European Union (ERC AdG SUBSTELLAR, GA 101054354). M.G. and E.J. are F.R.S-FNRS Senior Research Directors. TRAPPIST is funded by the Belgian Fund for Scientific Research (Fond National de la Recherche Scientifique, FNRS) under the grant FRFC 2.5.594.09.F, with the participation of the Swiss National

Science Fundation (SNF). R.B. acknowledges support from FONDECYT Project 1241963 and from ANID—Millennium Science Initiative—ICN12_009. M.K. acknowledges the support of the Natural Sciences and Engineering Research Council of Canada (NSERC), RGPIN-2024-06452. This research was funded by the Natural Sciences and Engineering Research Council of Canada (CRSNG), RGPIN-2024-06452. T.D. acknowledges support from the McDonnell Center for the Space Sciences at Washington University in St. Louis. We thank Adriana Kuehnel, who contributed to some of the PFS observations and who built and maintains the PFS website used for decision making of observations. A.J. acknowledges support from Fondecyt project 1251439.

Facilities: MAST (TESS), CTIO:1.5m, Max Planck:2.2m, CORALIE, Magellan:Clay, LCOGT, ExoFOP.

Software: AstroImageJ (K. A. Collins et al. 2017), Lightkurve (Lightkurve Collaboration et al. 2018), Tapir (E. Jensen 2013), Exofastv2 (J. D. Eastman et al. 2019).

ORCID iDs

Allyson Bieryla https://orcid.org/0000-0001-6637-5401
Karen A. Collins https://orcid.org/0000-0001-6588-9574
George Zhou https://orcid.org/0000-0002-4891-3517
David W. Latham https://orcid.org/0000-0001-9911-7388
Brad Carter https://orcid.org/0000-0003-0035-8769
Paul Dalba https://orcid.org/0000-0002-4297-5506
Robert Gagliano https://orcid.org/0000-0002-5665-1879
Thomas L. Jacobs https://orcid.org/0000-0003-3988-3245
Martti Holst Kristiansen https://orcid.org/0000-0002-2607-138X
Daryll LaCourse https://orcid.org/0000-0002-8527-2114
H.M. Schwengeler https://orcid.org/0000-0002-1637-2189
Khalid Barkaoui https://orcid.org/0000-0003-1464-9276
Rafael Brahm https://orcid.org/0000-0002-9158-7315
R. Paul Butler https://orcid.org/0000-0003-1305-3761
Douglas A. Caldwell https://orcid.org/0000-0003-1963-9616
Jeffrey D. Crane https://orcid.org/0000-0002-5226-787X
Tansu Daylan https://orcid.org/0000-0002-6939-9211
Sarah Deveny https://orcid.org/0009-0002-9833-0667
Jason D. Eastman https://orcid.org/0000-0003-3773-5142
Yadira S. Gaibor https://orcid.org/0000-0002-2036-2311
Michaël Gillon https://orcid.org/0000-0003-1462-7739
Thomas Henning https://orcid.org/0000-0002-1493-300X
Keith Horne https://orcid.org/0000-0003-1728-0304
Steve B. Howell https://orcid.org/0000-0002-2532-2853
Emmanuel Jehin https://orcid.org/0000-0001-8923-488X
Eric L. N. Jensen https://orcid.org/0000-0002-4625-7333
Andrés Jordán https://orcid.org/0000-0002-5389-3944
Michelle Kunimoto https://orcid.org/0000-0001-9269-8060
Colin Littlefield https://orcid.org/0000-0001-7746-5795
Léna Parc https://orcid.org/0000-0002-7382-1913
Samuel N. Quinn https://orcid.org/0000-0002-8964-8377
Malena Rice https://orcid.org/0000-0002-7670-670X
Joseph E. Rodriguez https://orcid.org/0000-0001-8812-0565
Richard P. Schwarz https://orcid.org/0000-0001-8227-1020
Ramotholo Sefako https://orcid.org/0000-0003-3904-6754
Stephen A. Shectman https://orcid.org/0000-0002-8681-6136
Avi Shporer https://orcid.org/0000-0002-1836-3120
Abderahmane Soubkiou https://orcid.org/0000-0002-0345-2147
Michal Steiner https://orcid.org/0000-0003-3036-3585
Marcelo Tala Pinto https://orcid.org/0009-0004-8891-4057
Johanna Teske https://orcid.org/0009-0008-2801-5040
Trifon Trifonov https://orcid.org/0000-0002-0236-775X
Cristilyn N. Watkins https://orcid.org/0000-0001-8621-6731
Sharon X. Wang https://orcid.org/0000-0002-6937-9034
Jhon Yana Galarza https://orcid.org/0000-0001-9261-8366
Samuel W. Yee https://orcid.org/0000-0001-7961-3907

References

Baraffe, I., & Chabrier, G. 2010, A&A, 521, A44
Baranne, A., Queloz, D., Mayor, M., et al. 1996, A&AS, 119, 373
Brahm, R., Jordán, A., & Espinoza, N. 2017, PASP, 129, 034002
Brown, T. M., Baliber, N., Bianco, F. B., et al. 2013, PASP, 125, 1031
Butler, R. P., Marcy, G. W., Williams, E., et al. 1996, PASP, 108, 500
Chatterjee, S., Ford, E. B., Matsumura, S., & Rasio, F. A. 2008, ApJ, 686, 580
Ciardi, D. R., Beichman, C. A., Horch, E. P., & Howell, S. B. 2015, ApJ, 805, 16
Collins, K. 2019, AAS Meeting, 233, 140.05
Collins, K. A., Kielkopf, J. F., Stassun, K. G., & Hessman, F. V. 2017, AJ, 153, 77
Crane, J. D., Shectman, S. A., & Butler, R. P. 2006, SPIE, 6269, 626931
Crane, J. D., Shectman, S. A., Butler, R. P., Thompson, I. B., & Burley, G. S. 2008, SPIE, 7014, 701479
Crane, J. D., Shectman, S. A., Butler, R. P., et al. 2010, SPIE, 7735, 773553
Cutri, R. M., Skrutskie, M. F., van Dyk, S., et al. 2003, yCat, 2246, 0
Cutri, R. M., Wright, E. L., Conrow, T., et al. 2021, yCat, 2328, 0
Dalba, P. A., Kane, S. R., Dragomir, D., et al. 2022, AJ, 163, 61
Dalba, P. A., Kane, S. R., Isaacson, H., et al. 2021, AJ, 161, 103
Dalba, P. A., Kane, S. R., Isaacson, H., et al. 2024, ApJS, 271, 16
Dong, J., Huang, C. X., Zhou, G., et al. 2021, ApJL, 920, L16
Dotter, A. 2016, ApJS, 222, 8
Doyle, L. R., Carter, J. A., Fabrycky, D. C., et al. 2011, Sci, 333, 1602
Eastman, J., Gaudi, B. S., & Agol, E. 2013, PASP, 125, 83
Eastman, J. D., Rodriguez, J. E., Agol, E., et al. 2019, arXiv:1907.09480
Eisner, N. L., Barragán, O., Aigrain, S., et al. 2020, MNRAS, 494, 750
Essack, Z., Dragomir, D., Dalba, P. A., et al. 2025, AJ, 170, 41
Ford, E. B., & Rasio, F. A. 2008, ApJ, 686, 621
Fortney, J. J., Marley, M. S., & Barnes, J. W. 2007, ApJ, 659, 1661
Furlan, E., & Howell, S. B. 2017, AJ, 154, 66
Furlan, E., & Howell, S. B. 2020, ApJ, 898, 47
Gaia Collaboration, Vallenari, A., Brown, A. G. A., et al. 2023, A&A, 674, A1
García-Mejía, J., de Beurs, Z. L., Tamburo, P., et al. 2025, arXiv:2506.20907
Gill, S., Bayliss, D., Cooke, B. F., et al. 2020, MNRAS, 491, 1548
Gillon, M., Jehin, E., Magain, P., et al. 2011, EPJWC, 11, 06002
Ginzburg, S., & Chiang, E. 2020, MNRAS, 498, 680
Guerrero, N. M., Seager, S., Huang, C. X., et al. 2021, ApJS, 254, 39
Gupta, A. F., Millholland, S. C., Im, H., et al. 2024, Natur, 632, 50
Hébrard, G., Bonomo, A. S., Díaz, R. F., et al. 2019, A&A, 623, A104
Heitzmann, A., Zhou, G., Quinn, S. N., et al. 2023, AJ, 165, 121
Hobson, M. J., Trifonov, T., Henning, T., et al. 2023, AJ, 166, 201
Høg, E., Fabricius, C., Makarov, V. V., et al. 2000, A&A, 355, L27
Howell, S. B., Everett, M. E., Sherry, W., Horch, E., & Ciardi, D. R. 2011, AJ, 142, 19
Howell, S. B., Martínez-Vázquez, C. E., Furlan, E., et al. 2025, FrASS, 12, 1608411
Jehin, E., Gillon, M., Queloz, D., et al. 2011, Msngr, 145, 2
Jenkins, J. M., Twicken, J. D., McCauliff, S., et al. 2016, SPIE, 9913, 99133E
Jensen, E. 2013, Tapir: A web interface for transit/eclipse observability, Astrophysics Source Code Library, ascl:1306.007
Kaufer, A., Stahl, O., Tubbesing, S., et al. 1999, Msngr, 95, 8
Kempton, E. M. R., Bean, J. L., Louie, D. R., et al. 2018, PASP, 130, 114401
Kristiansen, M. H. K., Rappaport, S. A., Vanderburg, A. M., et al. 2022, PASP, 134, 074401
Kurucz, R. L. 1993, SYNTHE Spectrum Synthesis Programs and Line Data (Smithsonian Astrophysical Observatory)
Laughlin, G. 2018, in Handbook of Exoplanets, ed. H. J. Deeg & J. A. Belmonte (Springer)

Lightkurve Collaboration, Cardoso, J. V. D. M., Hedges, C., et al. 2018, Lightkurve: Kepler and TESS Time Series Analysis in Python, Astrophysics Source Code Library, ascl:1812.013
Lindegren, L., Bastian, U., Biermann, M., et al. 2021, A&A, 649, A4
Mancini, L., Lillo-Box, J., Southworth, J., et al. 2016, A&A, 590, A112
Mann, C. R., Dalba, P. A., Lafrenière, D., et al. 2023, AJ, 166, 239
McCully, C., Volgenau, N. H., Harbeck, D.-R., et al. 2018, SPIE, 10707, 107070K
Naef, D., Latham, D. W., Mayor, M., et al. 2001, A&A, 375, L27
Nagasawa, M., Ida, S., & Bessho, T. 2008, ApJ, 678, 498
Paredes, L. A., Henry, T. J., Quinn, S. N., et al. 2021, AJ, 162, 176
Pepe, F., Mayor, M., Rupprecht, G., et al. 2002, Msngr, 110, 9
Petigura, E. A. 2015, PhD thesis, Univ. California, Berkeley
Petrovich, C., Tremaine, S., & Rafikov, R. 2014, ApJ, 786, 101
Queloz, D., Mayor, M., Weber, L., et al. 2000, A&A, 354, 99
Rasio, F. A., & Ford, E. B. 1996, Sci, 274, 954
Ricker, G. R., Winn, J. N., Vanderspek, R., et al. 2015, JATIS, 1, 014003
Sarkis, P., Mordasini, C., Henning, T., Marleau, G. D., & Mollière, P. 2021, A&A, 645, A79
Scott, N. J., Howell, S. B., Gnilka, C. L., et al. 2021, FrASS, 8, 138
Ségransan, D., Udry, S., Mayor, M., et al. 2010, A&A, 511, A45
Sing, D. K., Rustamkulov, Z., Thorngren, D. P., et al. 2024, Natur, 630, 831
Skrutskie, M. F., Cutri, R. M., Stiening, R., et al. 2006, AJ, 131, 1163
Smith, J. C., Stumpe, M. C., Van Cleve, J. E., et al. 2012, PASP, 124, 1000
Stassun, K. G., Oelkers, R. J., Pepper, J., et al. 2018, AJ, 156, 102
Stumpe, M. C., Smith, J. C., Catanzarite, J. H., et al. 2014, PASP, 126, 100
Stumpe, M. C., Smith, J. C., Van Cleve, J. E., et al. 2012, PASP, 124, 985
Teske, J. K., Thorngren, D., Fortney, J. J., Hinkel, N., & Brewer, J. M. 2019, AJ, 158, 239
Thorngren, D. P., Fortney, J. J., Murray-Clay, R. A., & Lopez, E. D. 2016, ApJ, 831, 64
Tokovinin, A., Fischer, D. A., Bonati, M., et al. 2013, PASP, 125, 1336
Welsh, W. F., Orosz, J. A., Carter, J. A., et al. 2012, Natur, 481, 475
Winn, J. N., Howard, A. W., Johnson, J. A., et al. 2009, ApJ, 703, 2091